TOWARD AN EMPIRICALLY-BASED PARAMETRIC EXPLOSION SPECTRAL MODEL

Sean R. Ford, William R. Walter, Stanley D. Ruppert, Eric M. Matzel, Teresa F. Hauk, and Rengin Gok

Lawrence Livermore National Laboratory

Sponsored by the National Nuclear Security Administration

Award No. DE-AC52-07NA27344/LL08-Parametrics-NDD02[1]

ABSTRACT

Small underground nuclear explosions need to be confidently detected and identified in regions of the world where they have never before occurred. We are developing a parametric model of the nuclear explosion seismic source spectrum derived from regional phases (Pn, Pg, Sn, and Lg) that is compatible with earthquake-based geometrical spreading and attenuation. Earthquake spectra are fit with a generalized version of the Brune spectrum, which is a three-parameter model that describes the long-period level, corner-frequency, and spectral slope at high-frequencies. Explosion spectra can be fit with similar spectral models whose parameters are then correlated with near-source geology and containment conditions. We observe a correlation of high gas-porosity (low strength) with increased spectral slope. However, there are trade-offs between the slope and corner-frequency, which we try to independently constrain using Mueller-Murphy relations and coda-ratio techniques. We complement our previous work that focused on the Nevada National Security Site (NNSS, formerly the Nevada Test Site) with data from explosions at the Semipalatinsk Test Site recorded at the Borovoye Geophysical Observatory (BRV). The BRV data archive allows for application of the parametric explosion model in a high-strength near-source geology. The relationship between the parametric equations and the geologic and containment conditions will assist in our physical understanding of the nuclear explosion source. The achievable goal of our parametric model development is to be able to predict observed local and regional distance seismic amplitudes for event identification and yield determination in regions with incomplete or no prior history of underground nuclear testing.

Report Documentation Page

Form Approved
OMB No. 0704-0188

1. REPORT DATE **SEP 2011**	2. REPORT TYPE	3. DATES COVERED **00-00-2011 to 00-00-2011**
4. TITLE AND SUBTITLE **Toward an Empirically-Based Parametric Explosion Spectral Model**		5a. CONTRACT NUMBER
		5b. GRANT NUMBER
		5c. PROGRAM ELEMENT NUMBER
6. AUTHOR(S)		5d. PROJECT NUMBER
		5e. TASK NUMBER
		5f. WORK UNIT NUMBER
7. PERFORMING ORGANIZATION NAME(S) AND ADDRESS(ES) **Lawrence Livermore National Laboratory,7000 East Ave,Livermore,CA,94550-9234**		8. PERFORMING ORGANIZATION REPORT NUMBER
9. SPONSORING/MONITORING AGENCY NAME(S) AND ADDRESS(ES)		10. SPONSOR/MONITOR'S ACRONYM(S)
		11. SPONSOR/MONITOR'S REPORT NUMBER(S)

12. DISTRIBUTION/AVAILABILITY STATEMENT
Approved for public release; distribution unlimited

13. SUPPLEMENTARY NOTES
Published in the Proceedings of the 2011 Monitoring Research Review - Ground-Based Nuclear Explosion Monitoring Technologies, 13-15 September 2011, Tucson, AZ. Volume I. Sponsored by the Air Force Research Laboratory (AFRL) and the National Nuclear Security Administration (NNSA). U.S. Government or Federal Rights License

14. ABSTRACT
Small underground nuclear explosions need to be confidently detected and identified in regions of the world where they have never before occurred. We are developing a parametric model of the nuclear explosion seismic source spectrum derived from regional phases (Pn, Pg, Sn, and Lg) that is compatible with earthquake-based geometrical spreading and attenuation. Earthquake spectra are fit with a generalized version of the Brune spectrum, which is a three-parameter model that describes the long-period level, corner-frequency, and spectral slope at high-frequencies. Explosion spectra can be fit with similar spectral models whose parameters are then correlated with near-source geology and containment conditions. We observe a correlation of high gas-porosity (low strength) with increased spectral slope. However, there are trade-offs between the slope and corner-frequency, which we try to independently constrain using Mueller-Murphy relations and coda-ratio techniques. We complement our previous work that focused on the Nevada National Security Site (NNSS, formerly the Nevada Test Site) with data from explosions at the Semipalatinsk Test Site recorded at the Borovoye Geophysical Observatory (BRV). The BRV data archive allows for application of the parametric explosion model in a high-strength near-source geology. The relationship between the parametric equations and the geologic and containment conditions will assist in our physical understanding of the nuclear explosion source. The achievable goal of our parametric model development is to be able to predict observed local and regional distance seismic amplitudes for event identification and yield determination in regions with incomplete or no prior history of underground nuclear testing.

15. SUBJECT TERMS					
16. SECURITY CLASSIFICATION OF:			17. LIMITATION OF ABSTRACT	18. NUMBER OF PAGES	19a. NAME OF RESPONSIBLE PERSON
a. REPORT **unclassified**	b. ABSTRACT **unclassified**	c. THIS PAGE **unclassified**	**Same as Report (SAR)**	**11**	

Standard Form 298 (Rev. 8-98)
Prescribed by ANSI Std Z39-18

OBJECTIVES

We aim to develop a practical explosion source parametric spectral model, based on all available data, that describes nuclear explosion *P*- and *S*-wave source spectra for a variety of geologic and containment conditions. This approach follows the simple earthquake parametric spectral model based on Brune (1970), which is used for the MDAC approach (Walter and Taylor, 2001) to improve earthquake/explosion discrimination. In regions without prior explosions, the parametric model could be combined with earthquake-derived path corrections to predict explosion regional phase amplitudes, improve discriminants such as *P*/*S* ratios, and support identification procedures (e.g., Event Categorization Matrix, [ECM]) that explicitly need to use explosion discriminant probability density functions.

It is well known that depth and near-source material properties can affect seismic estimates of explosion yield, and prior work at the NNSS (e.g., Walter et al., 1995) has found that explosions in weak materials have lower corner frequencies and steeper spectral fall-offs for *P*-waves than is predicted by the standard Mueller and Murphy (1971) model. As part of this research, we hope to quantify these effects as a function of frequency and wave type. Additionally, many of the most effective regional discriminants (high-frequency *P*/*S* ratios) make use of *S*-waves, as do *S*-wave coda yield estimation techniques, yet there remain many questions about how to predict explosion *S*-wave amplitudes. The development of a combined *P*- and *S*-wave spectral model consistent with observed regional *P*-and *S*-wave data is an objective of this work.

RESEARCH ACCOMPLISHED

Introduction

In previous work that looked at low to high frequency ratios of regional phase (e.g., *Pn*, *Pg*, *Lg*) amplitudes to separate explosions from earthquakes at NNSS, Walter et al. (1995) noted that the results showed a strong dependence on the source media properties. Nuclear tests in weak and/or high gas porosity media tended to have higher values and discriminate better from earthquakes than explosions in stronger and/or lower gas porosity media.

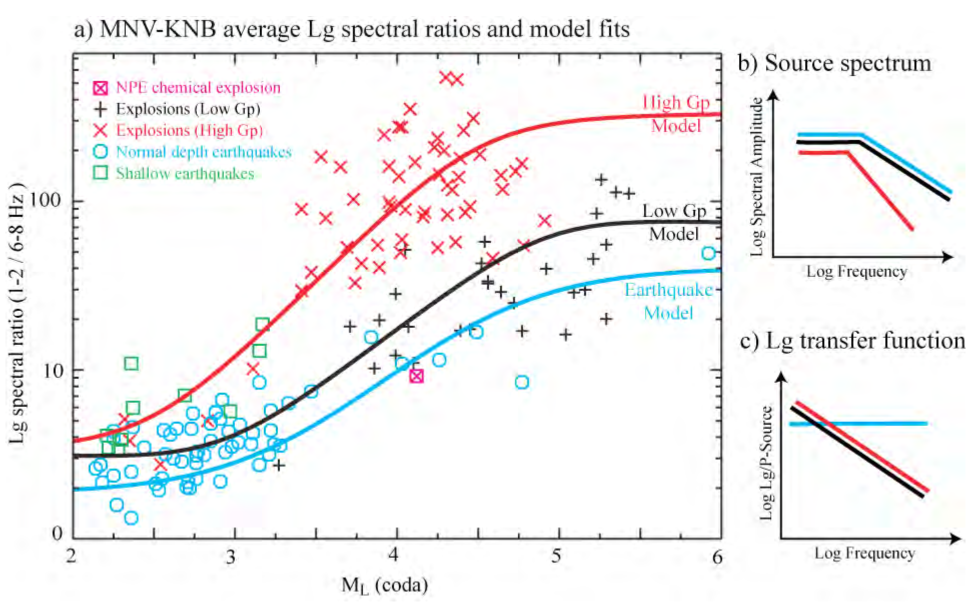

Figure 1. Simple first-order source model fits to low to high frequency spectral ratios of *Lg* amplitudes from Walter et al. (1995, Figure 8). Earthquake displacement spectra are fit with the Brune (1970) model (blue line), which is constant at low frequencies and falls off above a corner frequency as f^{-2}. Explosions are fit with two extremes of the Denny and Goodman (1990) model in order to investigate explosion dependence on emplacement material (namely, gas porosity [*Gp*]). The 'Low *Gp*' model (black line) has an effective fall-off similar to the earthquake model. The 'High *Gp*' model (red line) has a greater fall-off of f^{-3}.

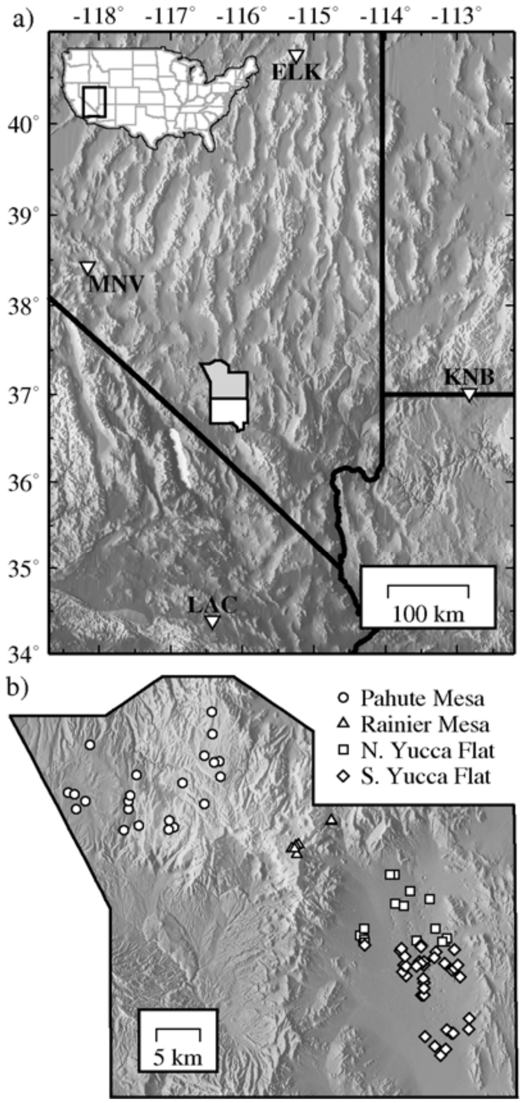

Figure 2. a) Regional map of stations used in the analysis. The location of the map within the continental US is given by the inset map. The NNSS is outlined and the shaded section is shown in (b). b) Map of the northern NNSS with explosion locations and Vergino and Mensing (1990) area designations.

For example, in Figure 1 the ratio of the *Lg* amplitude at 1–2 Hz compared with the amplitude at 6–8 Hz is shown as a function of magnitude. The earthquakes (blue circles and green squares) show the expected trend with magnitude going from a low value for small events when the corner frequency is above 8 Hz and both measurements are on the constant part of the source spectra that is proportional to moment. For large magnitudes, the source corner frequency drops below 1 Hz and then both measures are on the part of the source spectra that decays with frequency as f^{-2}, resulting in high spectral ratio values. As magnitude increases, the earthquakes follow a sigmoid curve as shown by the blue line, which is based on the Brune (1970) model. The explosions are split into two categories based on the source media, a high gas porosity (*Gp*) and low strength (defined as $\rho\alpha^2$, where ρ is density and α is the local compressional wave speed) group (red x) and low *Gp* high strength group (black crosses), and a clear difference between the two can be seen. In fact, the low *Gp* explosions reach spectral ratio values that imply much steeper falloff than f^{-2}.

To fit the explosion data, we used two extremes of the Denny and Goodman explosion model (1990), which has two corner frequencies. In the low *Gp* case we allowed the second corner to be at a higher frequency than the range of interest, giving an effective f^{-2} falloff. In the high *Gp* case we forced the corners to be the same, giving an f^{-3} falloff. In both cases we used the observed 3 Hz corner frequency of the 1993 Non-Proliferation Experiment (NPE), a kiloton chemical explosion and assumed the corner frequency scales with the cube root of M_L(coda). Given that a pure explosion should not generate *S*-waves, one way to think about the *Lg* spectral ratio is as the product of the *P*-wave source ratio and a transfer function ratio, where the transfer function is a representation of how efficiently the source generated *P*-waves are converted (by whatever means) into *S*-waves. We estimated the transfer function ratio as a function of frequency as shown in Figure 1, and then multiplied the *P*-wave based Denny-Goodman model curves by these factors and then compared them to the *Lg* spectral ratio in Figure 1. The result is a fairly reasonable first order fit to the data. Interestingly, since the explosion *Lg* transfer functions are larger than those for the earthquakes, it shifts the explosion *Lg* spectral ratios to relatively higher values than for the earthquakes, improving the discrimination performance of *Lg* spectral ratios over those of *Pn* alone (Walter et al. 1995, Figure 7).

While in this case, the Denny and Goodman (1990) model provides a reasonable fit to these NNSS data, it is not clear how we would use it in other regions. Furthermore the limitation of only two choices of high frequency fall-off does not capture the full range of the observations. To develop a practical parametric source spectral model we want to be able to tie parameters like low-frequency level, corner-frequency and fall-off rate to measureable

Table 1. NNSS regional attenuation and geometric spreading parameters.

Phase	η	r_0 (km)	Q_0	γ
Pn	1.1	0.001	210	0.65
Pg	0.5	100	190	0.45
Lg	0.5	100	200	0.54

properties like yield, depth, and media properties such as gas porosity, water content, and strength. In the next section we take a more general approach to fitting the NNSS explosion data with a simple spectral model parameterized by a long-period level, corner-frequency, and high-frequency roll-off.

Data and Methods

We employ the NNSS explosion dataset of Walter et al. (2004), specifically the raw spectra of that dataset. Waveforms are de-meaned, de-trended and instrument corrected to acceleration. The signal is windowed with a 5% cosine taper that starts before the pick, where the time before the pick is 5% of the total time window. The Fourier transform is calculated and displacement spectra are obtained via double integration in the frequency domain. Finally, the resultant amplitude spectra are interpolated and smoothed to obtain a sampling period of 0.05 $\log_{10}$ Hz.

Spectra of each seismic phase for each explosion are calculated from the recordings of stations of the Livermore NNSS Network, ELK (Elko, NV), KNB (Kanab, UT), LAC (Landers, CA), and MNV (Mina, NV). The locations of these stations relative to the NNSS are given in Figure 2. These spectra are then corrected for geometrical spreading and regional, frequency-dependent attenuation of the form $Q = Q_0 f^{\gamma}$, where Q_0 is Q at 1 Hz and γ is the power-law dependence on frequency, f. We employ the Street et al. (1975) parametric form of geometrical spreading,

$$G(r) = \begin{cases} r^{-1}, & r < r_0 \\ 1/r_0 (r_0/r)^{\eta}, & r \geq r_0 \end{cases}, \tag{1}$$

where r_0 is the distance at which the spreading transitions from spherical- to a cylindrical-type spreading and η is the distance dependence. The attenuation and spreading model parameters for each seismic phase are given in Table 1.

We require three of the four stations listed above to have recorded an event with a signal-to-noise ratio greater than two. We also inspect each spectra for non-stationary noise at high-frequency (typically >9 Hz) due to multi-band recording problems and restrict spectral fitting to bands unaffected by problems. The spectra are jointly fit with a simple parametric form given by

$$S(f) = \frac{S_0}{1 + (f/f_c)^{\psi}}, \tag{2}$$

in a least-squares inversion that also provides standard error for each parameter estimate. Equation (2) describes the simplest behavior expected for seismic spectra. It has a constant level at low frequencies (S_0), which is proportional to

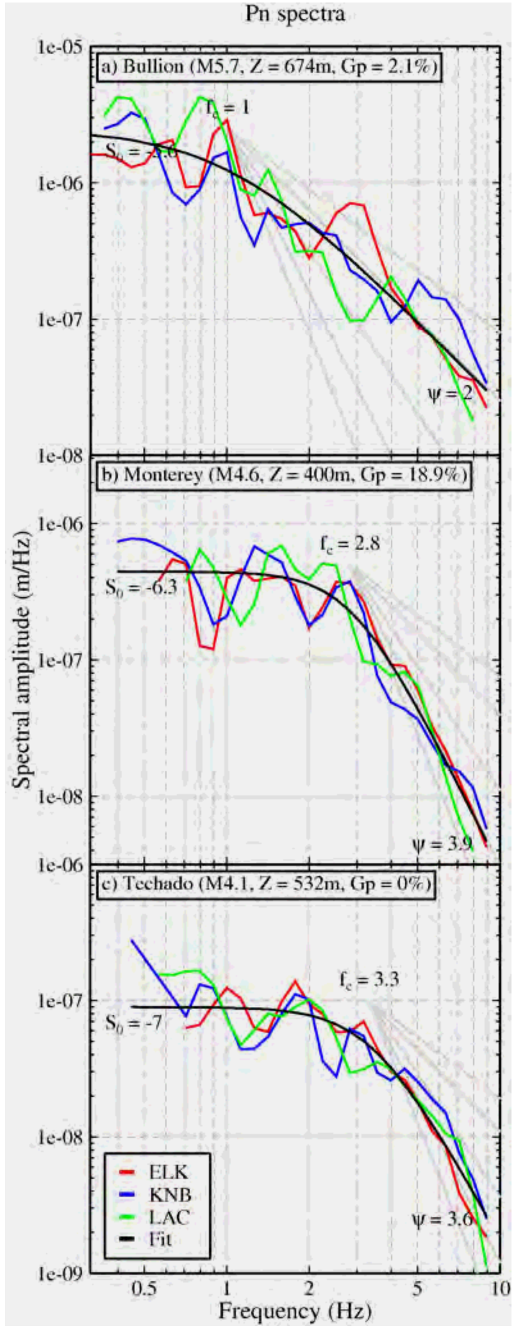

Figure 3. ***Pn* spectra examples with the name, magnitude (where $M = m_b[Pn]$), depth (Z), and gas porosity (Gp) given in the subtitles. The long-period level (S_0), corner-frequency (f_c), and fall-off (ψ) are given in each plot, and the spectra are colored by station and the fit is shown in the legend in the lowermost plot. a) Spectra for an event with low *Gp* and ω^{-2} fall-off. b) Spectra for an event with high *Gp* and high fall-off. c) Spectra for an event with low *Gp* and high fall-off.**

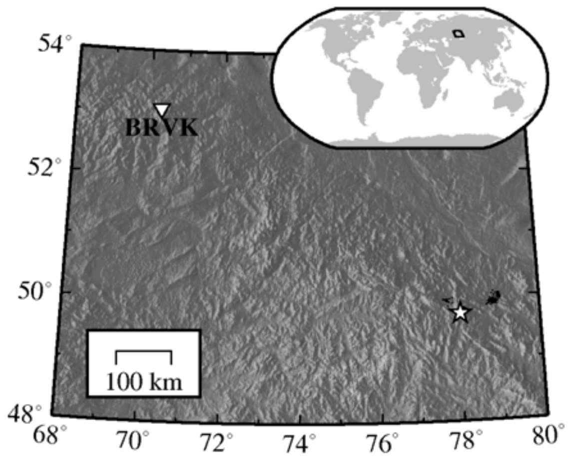

Figure 4. Regional map of station in Borovoye (BRVK) and recorded events in the archive (dots) along with the event shown in Figure 5 (star). The location of the map is given in the inset global map.

static displacement, and falls off at high frequencies with a slope of $f^{-\psi}$ beyond a corner frequency f_c. Examples of the spectra and model fits are proportional to static displacement, and fall off at high frequencies with a slope of $f^{-\psi}$ beyond a corner frequency f_c. Examples of the spectra and model fits are given in Figure 3. BULLION (Figure 3a) is fit well with a standard f^{-2} (ψ=2) spectral fall-off, but MONTEREY (Figure 3b), detonated in weak material, requires a steeper fall-off where the best fit $\psi \approx 4$.

We are complementing the NNSS dataset with the Borovoye (BRV) archive that has recently been deglitched and response functions estimated (Richards and Kim, 2009). This archive provides about 200 recordings of explosions at Semipalatinsk Test Site of the former Soviet Union (Figure 4). As an example, we plot the regional phase spectra of one of the explosions mapped in Figure 4 (shown by a star) in Figure 5. The attenuation and spreading model parameters used to correct these spectra are given in Table 2. Pn parameters are from Walter and Priestley (1991) and Pg and Lg are from Priestley et al. (1990). We plan to complement these initial models with data from earthquakes in the region recorded at BRV. The regional phase spectra are fit with $\psi \approx 2$.

The BRV regional seismic phase spectra, especially *Pn* and *Pg* (Figure 5a-b), show the trade-off in fitting the corner frequency and the roll-off. Attempts to diminish this trade-off will be discussed in the next section.

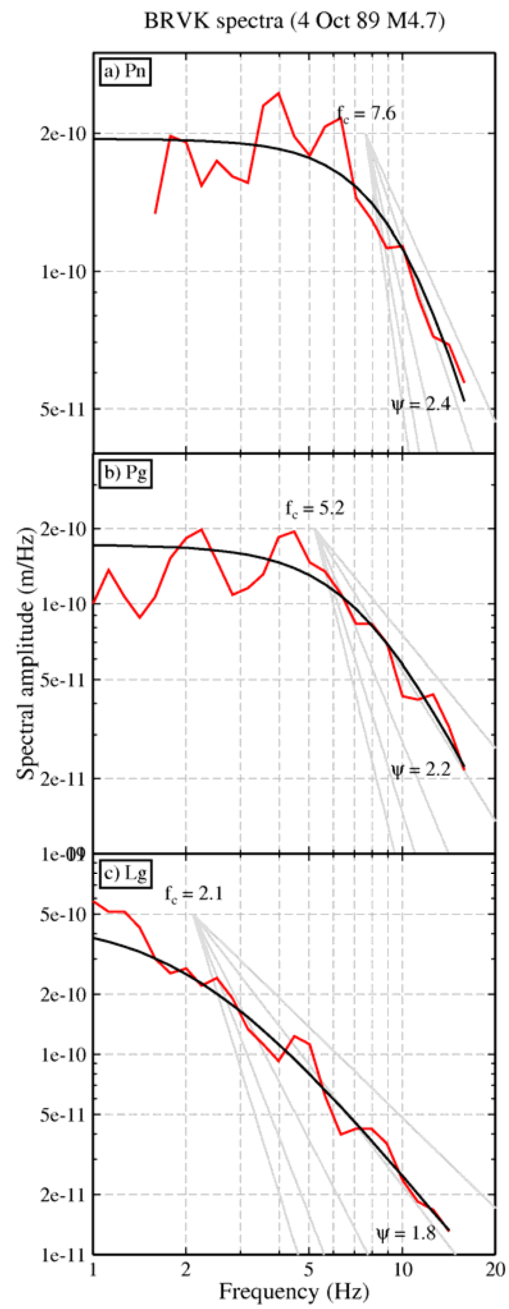

Figure 5. *Pn* spectra of example BRVK event (shown by star in Figure 4). Values given in each plot are defined in Figure 3.

Preliminary Results

Previous results (Ford et al., 2010) showed that there is a correlation between corner-frequency and fall-off that is most probably related to the least-squares fitting of Equation (2) and not to any physical relationship. The trade-off could produce biased estimates of ψ, so we seek to constrain f_c in Equation (2) using the corner frequency predicted by Denny and Johnson (1991), $f_c^{D\&J}$.

Table 2. BRV regional attenuation and geometric spreading parameters

Phase	η	r_0 (km)	Q_0	γ
Pn	1.1	0.001	300	0.50
Pg	0.5	100	825	0.48
Lg	0.5	100	367	0.48

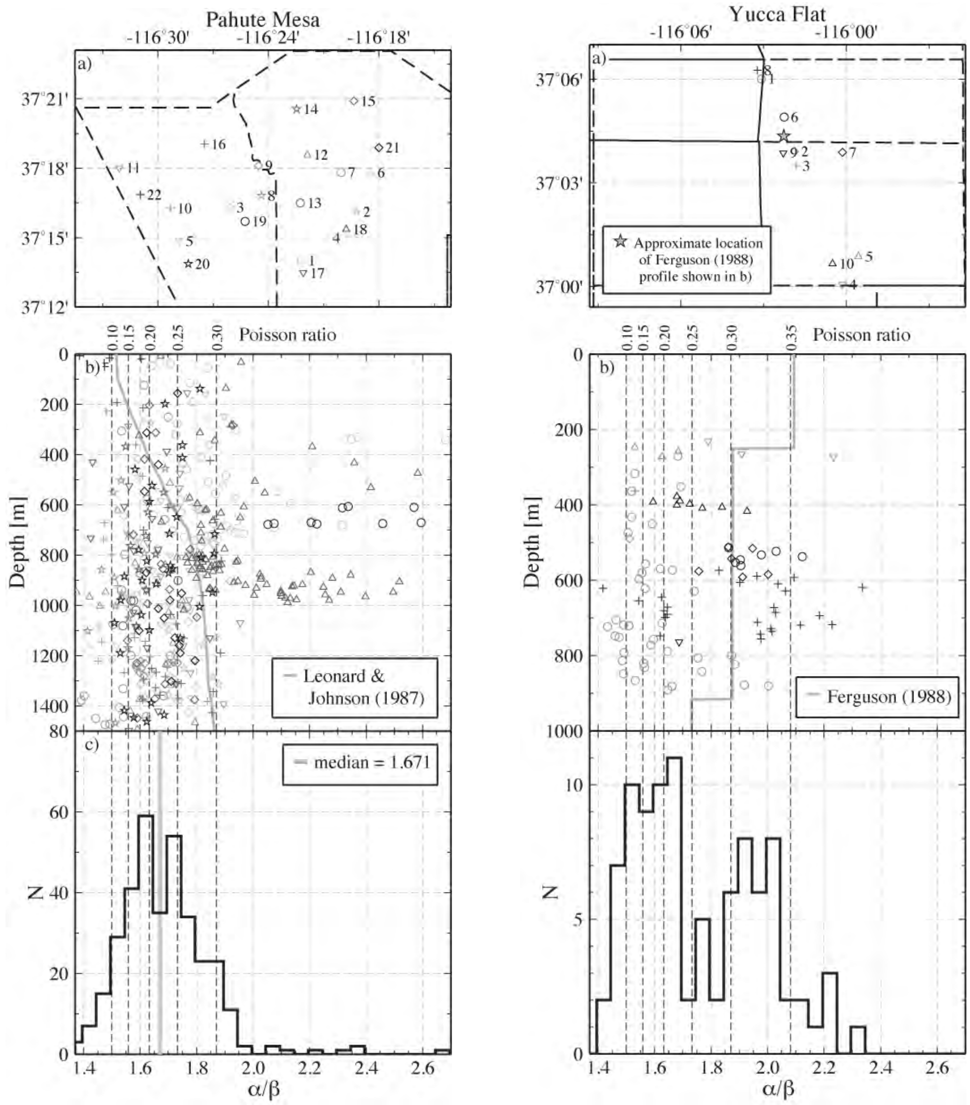

Figure 6. Analysis of Vp/Vs (α/β) ratio from USGS database (Wood, 2007) at Pahute Mesa and Yucca Flat. The ratio as a function of depth from Leonard and Johnson (1987) and Ferguson (1988) are shown for Pahute Mesa and Yucca Flat, respectively. Based on the distribution, we estimate constant Vp/Vs ratios of 1.671 and 1.871 (ν = 0.3) at Pahute Mesa and Yucca Flat, respectively.

In order to obtain the shear modulus and shear velocity values used in the Denny and Johnson (1991) relationships we had to convert working-point compressional velocities. We used the USGS database of Wood (2007) to find appropriate Vp/Vs or Poisson ratios. Figure 6 shows the analysis at Pahute Mesa, where an average Vp/Vs ratio of 1.671 is estimated, and Yucca Flat, where an average Vp/Vs ratio of 1.871 (ν=0.3) is estimated. We set $f_c = f_c^{D\&J}$ in Equation (2) and estimate ψ. ψ is still correlated with f_c, but it is now less due to the fitting procedure. Comparisons of spectral fall-off (ψ) with various geophysical parameters are given in Figure 7.

We perform a comprehensive search for material property correlation with ψ, using several regressions on ψ for water content (S_W), gas porosity (Gp), density (ρ), compressional wave speed (α), compressional modulus ($M=\rho\alpha^2$), and scaled depth-of-burial (sDOB = depth/yield$^{1/3}$). These geophysical parameters are taken from the database of

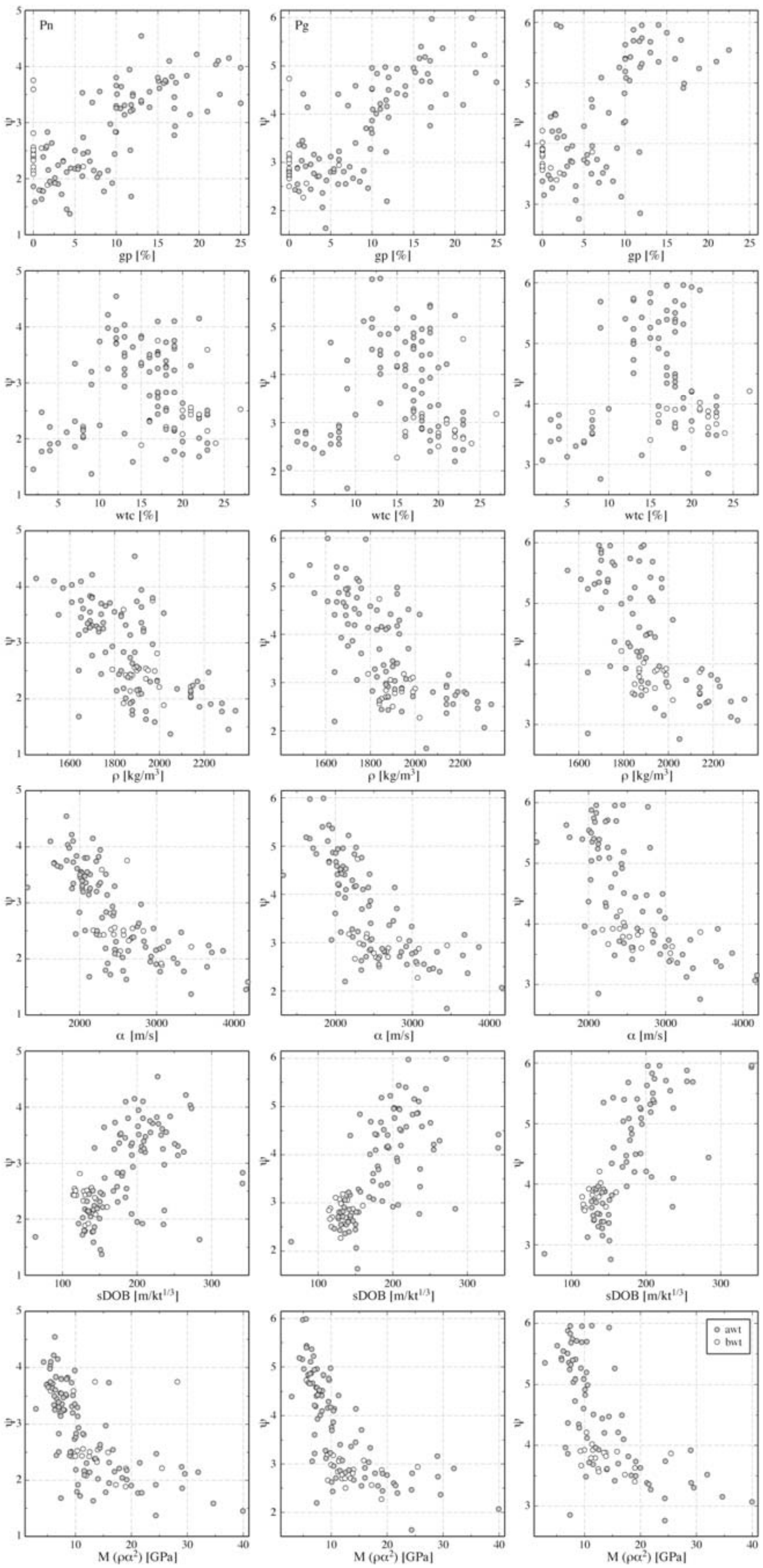

Figure 7. Spectral falloff (ψ) of Pn, Pg, and Lg (1st, 2nd, and 3rd columns, respectively) versus geophysical parameters at explosion working point from Springer et al. (2002). Slight correlations can be found for gas porosity (gp), density (ρ), velocity (α), scaled depth-of-burial (sDOB), and compressional modulus (M = $\rho\alpha^2$). Water content (wtc) shows little correlation. Explosions above and below the water table (awt and bwt, respectively) are given by the filled and open circles, respectively. The location of an explosion placed above or below the water table affects the correlation with gp, but not so much for the other parameters. The relationship of ψ to α (and therefore also M) is more power-law than linear, or linear up to a certain value and then flat (constant ψ). The correlated parameters are used in a linear regression to find the best parametric model for ψ for each seismic phase.

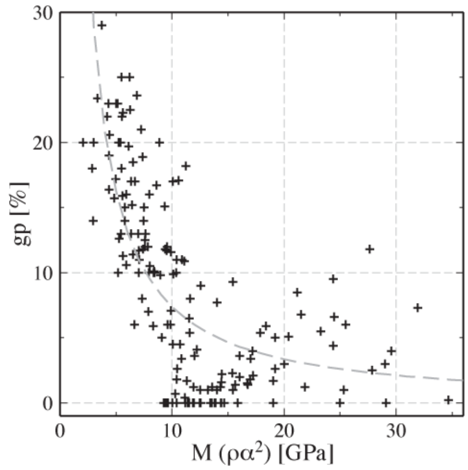

Figure 8. From Springer et al. (2002) we find a good proxy for gas porosity (gp) is a power-law relationship with compressional modulus. The dashed line is gp = 100M$^{-1.135}$.

Springer et al. (2002) and are reported to represent an integrated value over the source region. Yield was inferred from $m_b(Pn)$ based on the Vergino and Mensing (1990) relationship at NNSS. Figure 7 shows the dependence of ψ on these parameters. Events below the water table do not follow the trend of increased ψ with *Gp* (open circles in Figure 7), so saturation reduces the linearity of the dependence. We quantify the saturation effect with a parameter that measures the portion of the whole elastic volume that is below the water table, S_V, which ranges from 0 (completely above the water table) to 1 (completely below the water table).

Using a step-wise regression criteria we found the most significant parameters in a linear regression model to be *M*, *Gp*, and sDOB. We then perform a least-squares regression using these parameters weighted by the estimated inverse variance of ψ. The model is given by the equation below and the parameters in the Table 3.

$$\psi = \beta_0 - \beta_1 sDOB + \beta_2 Gp + \beta_3 S_V + \beta_4 M. \qquad (3)$$

In new testing environments geophysical parameters such as gas porosity will be difficult to obtain. Using NNSS geophysical data from Springer et al. (2002) we find that *Gp* is best approximated by a power-law relationship to the compressional modulus ($M = \rho\alpha^2$) shown in Figure 8 and given by $Gp = 100M^{-1.135}$, where the compressional modulus is in GPa.

Table 3. Parameters for Eq (3)

Type	β_0	β_1	β_2	β_3	β_4
Pn	2.35	3.6	42.6	−2.2	−40.0
Pg	2.96	5.5	57.2	−7.3	−45.7
Lg	3.35	9.1	39.3	−4.9	−46.6

Inspired by Murphy & Bennett (2010), we analyze the *Pn* spectra of groups of nearby events (pairwise distance < 10 km). Possible groups are shown in Figure 9. The analysis here uses the grouping marked by yellow inverted triangles in Figure 9.

These spectra are then corrected to a common source. In this case, we use an explosion with a corner frequency ~1 Hz. These parameters are estimated with the relationships given by Denny & Johnson (1991). The spectra are then placed in one of three groups; (1) below the water table, (2) above the water table with gas porosity < 12%, and (3) above the water table with gas porosity > 12%.

We find the average spectra of each of these three groups and then calculate the ratios of those average spectra to see how spectral-slope may be different between them. The spectra, their averages and ratios are given in Figure 10. In this case, at frequencies greater than the corner there is an increase in falloff slope of about 2 for the above-the-water-table-with GP > 12 % average compared to the others. This effect can be seen at MNV, KNB, and ELK. This ratio difference could be due to an increased slope of low-strength (high gas porosity) spectra as was found in the individual spectral analysis using many explosions. The difference in slope between the two populations is near 2, as seen by the comparison with the dashed line in Figure 10.

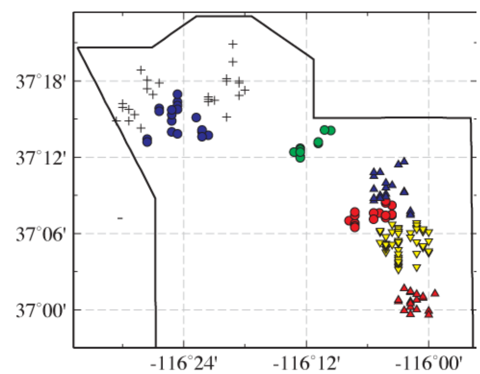

Figure 9. Possible groupings (colored symbols) of explosions at NNSS (outline) where the pairwise distance between explosions is < 10 km. The analysis here uses the group marked by the yellow inverted triangles.

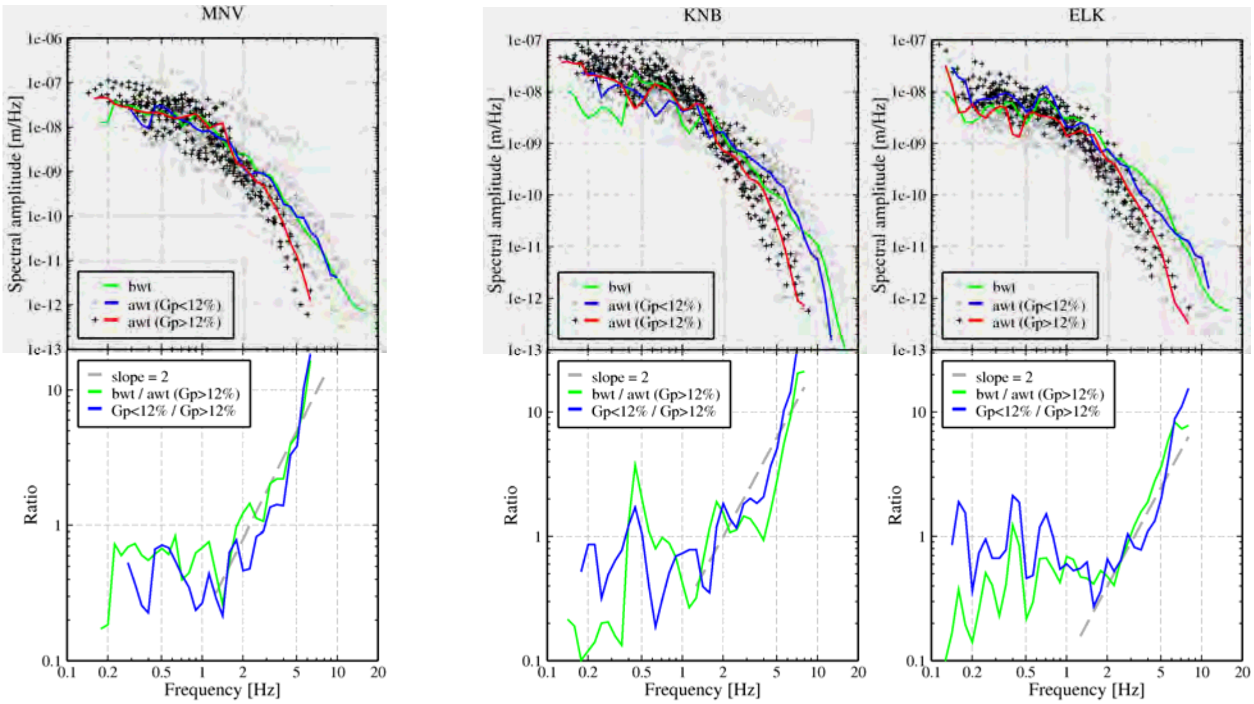

Figure 10. Pn spectral ratio analysis. First row, spectra grouped by below the water table (bwt, light gray crosses), above the water table with gas porosity < 12% (awt Gp<12%, gray crosses), and above the water table with gas porosity > 12% (awt Gp>12%, black crosses). The averages of these grouped spectra are given by the colored lines. Second row, ratios of the averages are calculated. The ratios of bwt and awt (Gp<12%) to awt (Gp>12%) given by the green and blue lines, respectively, show an increased slope beginning near the corner frequency. The dashed gray line has slope of 2 and begins at 1 Hz.

CONCLUSIONS AND RECOMMENDATIONS

Our preliminary analysis of regional phase spectra of NNSS explosions shows that a simple spectral model with variable fall-off is appropriate, and the fall-off correlates well with the material properties, gas porosity, compressional modulus, and saturation volume, as well as the scaled depth-of-burial. A linear model for each phase dependent on these parameters is given by equation (3). In regions where gas porosity is unknown, the compressional modulus may be a suitable proxy. Ratios of groups of events where one group are events in high gas porosity (Gp>12%) material show that spectral fall-off is greater for the weaker material events.

This initial *P*-wave spectral fitting focused on correlating material properties with the model parameters. We will perform similar analyses for spectra at Borovoye. The comparison of seismic phases with NNSS results will allow for an examination of *P/S* scaling relationships, which can be compared with results from the Fisk (2007) study at NNSS. The results of this study with a variable fall-off spectral model will be compared with other spectral models (e.g., Denny and Johnson [1991] and references therein). In addition, we will formally analyze the error and trade-offs in the estimated parameters of Equation (2). Finally, we hope that through parametric modeling we may gain insight to the physical model underlying these observations.

REFERENCES

Baker, D., W.-Y. Kim, H. Patton, G. Randall, and P. Richards (2009). Improvements to a major digital archive of seismic waveforms from nuclear explosions: The Borovoye seismogram archive, in *Proceedings of the 2009 Monitoring Research Review: Ground-Based Nuclear Explosion Monitoring Technologies,* LA-UR-09-05276, Vol. 1, pp. 12–21.

Brune, J. N. (1970). Tectonic stress and the spectra of seismic shear waves from earthquakes, *J. Geophys. Res.* 75: 4997–5009.

Denny, M. D. and D. M. Goodman (1990). A case study of the seismic source function; SALMON and STERLING reevaluated, *J. Geophys. Res.* 95: 19705–19723.

Denny, M. D. and L. R. Johnson (1991). The explosion seismic source function: Models and scaling laws reviewed, in *Explosion Source Phenomenology*, eds. Taylor S. R. et al., AGU Monograph 65: 1–24.

Ferguson, J. F. (1988). Body-wave magnitude variation at Yucca Flat, Nevada, *Bull. Seismol. Soc. Am.* 78: 863–872.

Fisk, M. D. (2007). Corner frequency scaling of regional seismic phases for underground nuclear explosions at the Nevada Test Site, *Bull. Seismol. Soc. Am.* 97: 977–988.

Ford, S. R., W. R. Walter, S. R. Ruppert, E. M. Matzel, T. F. Hauk, and M. R. Gok (2010). Toward an empirically-based parametric explosion spectral model, in *Proceedings of the 2010 Monitoring Research Review: Ground-Based Nuclear Explosion Monitoring Technologies*, LA-UR-09-05276, Vol. 1, pp. 12–21.

Goldstein, P., S. P. Jarpe, K. M. Mayeda, and W. R. Walter (1994). Separation of source and propagation effects and regional distances, in *Proceedings of the Symposium on the Non-Proliferation Experiment: Results and Implications for Test Ban Treaties*, DOE-CONF-9404100, 6-272–6-276.

Leonard, M. A., and L. Johnson (1987). Velocity structure of Silent Canyon Caldera, Nevada Test Site, *Bull. Seismol. Soc. Am.* 77: 597-613.

Mueller, C. S. and J. R. Murphy (1971). Seismic characteristics of underground nuclear detonations, Part I: Seismic spectrum scaling, *Bull. Seismol. Soc. Am.* 61: 1675–1692.

Murphy, J. and Bennett (2010). An Analysis of the Seismic Source Characteristics of Explosions in Low-Coupling Dry Porous Media in *Proceedings of the 2010 Monitoring Research Review: Ground-Based Nuclear Explosion Monitoring Technologies,* LA-UR-09-05276, Vol. 1, pp. 12–21.

Priestley, K. F., W. R. Walter, V. Martynov, and M. V. Rozhkov (1990). Regional seismic recordings of the soviet nuclear explosion of the Joint Verification Experiment, *Geophys. Res. Lett.* 17(2): 179–82.

Stevens, J. L. and S. M. Day (1985). The physical basis of m_b:M_S and variable frequency magnitude methods for earthquake/explosion discrimination, *J. Geophys. Res.* 90: 3009–3020.

Street, R. L., R. B. Herrmann, and O. W. Nuttli (1975). Spectral characteristics of the Lg wave generated by central United States earthquakes, *Geophys. J. R. Astro.* 41: 51–63.

Vergino, E. S. and R. W. Mensing (1990). Yield estimation using regional mb(Pn), *Bull. Seismol. Soc. Am.* 80: 656–674.

Walter, W. R, K. D. Smith, J. L. O'Boyle, T. F. Hauk, F. Ryall, S. D. Ruppert, S. C. Myers, R. Abbot, and D. A. Dodge (2004). An assembled western United States dataset for regional seismic analysis, *Lawrence Livermore National Laboratory* document, UCRL-TR-206630.

Walter, W. R. and S. R. Taylor (2001). A revised magnitude and distance amplitude correction (MDAC2) procedure for regional seismic discriminants, *Lawrence Livermore National Laboratory* document, UCRL-ID-146882.

Walter, W. R., K. M. Mayeda, and H. J. Patton (1995). Phase and spectral ratio discrimination between NTS earthquakes and explosions, Part 1: Empirical observations, *Bull. Seimol. Soc. Am.* 85: 1050–1067.

Walter, W. R. and K. F. Priestley (1991). Explosion Source Phenomenology. AGU monograph

Wood, D. B. (2009). Digitally available interval-specific rock-sample data compiled from historical records, Nevada Test Site and vicinity, Nye County, Nevada, USGS Data Series 297.